The Eurasia Proceedings of Science, Technology, Engineering & Mathematics (EPSTEM)
ISSN: 2602-3199

The Eurasia Proceedings of Science, Technology, Engineering and Mathematics (EPSTEM), 2025

Volume 38, Pages 226-243

IConTES 2025: International Conference on Technology, Engineering and Science

Computational Materials Design: Tuning Optoelectronic Response in GaxIn1-xBiyP1-y Alloys via Structural Matching to InP

Malika Tehami
Djillali Liabes University of Sidi Bel Abbes

Miloud Benchehima
University of Sciences and Technology

Hamza Abid
Djillali Liabes University of Sidi Bel Abbes

Abstract: This theoretical study presents a computational investigation into the structural, electronic, and optical properties of GaxIn1-xBiyP1-y quaternary alloys specifically lattice-matched to an InP substrate, utilizing density functional theory (DFT). The calculations were performed using the full-potential linearized augmented plane wave (FP-LAPW) method. Structural properties were assessed using the local density approximation (LDA) and the Wu-Cohen generalized gradient approximation (WC-GGA), with WC-GGA used to define the lattice-matching target based on the calculated InP lattice constant. Electronic properties were determined using the Engel-Vosko GGA (EV-GGA) and Tran-Blaha modified Becke-Johnson (TB-mBJ) functionals. Optical properties were analyzed in detail, with optical band gaps derived using Tauc's method. Lattice-matching conditions to InP were established, yielding calculated lattice constants around 5.9 Å for matched compositions (x, y), in excellent agreement with the experimental InP value (5.869 Å). Band structure analysis confirms these alloys are direct band gap semiconductors at the Γ point for all studied lattice-matched compositions. The investigation of optical properties reveals that the electronic band gaps (via TB-mBJ) correspond to wavelengths spanning approximately 0.91 µm to 2.46 µm, while Tauc analysis yields optical band gaps corresponding to ~0.9 µm to ~1.56 µm, all while maintaining lattice matching. These findings highlight GaxIn1-xBiyP1-y/InP alloys as promising materials for optoelectronic devices, particularly for telecommunication applications operating at 1.3 µm and 1.55 µm, due to their tunable optoelectronic characteristics and structural compatibility with InP.

Keywords: GaInBiP quaternary alloys, Density functional theory, Lattice matching, Optoelectronic properties, Optical communication

Introduction

In recent years, great efforts have been made in the research of semiconductor alloys and nanostructures containing bismuth (Bi). These new Bi-containing alloys and nanostructures possess interesting physical properties and reveal promising device applications (Zhang et al., 2019), (Wang et al., 2019), (Paulauskas et al., 2020), (Usman et al., 2019), (Donmez et al., 2021), (Jain et al., 2022). The incorporation of Bi into traditional III-V compounds leads to substantial modifications in electronic band structure, most notably a strong reduction in the band gap energy and an increase in spin-orbit splitting (Paulauskas et al., 2020). The GaxIn1-xBiyP1-y quaternary alloy system, composed of Indium (In), Gallium (Ga), Phosphorus (P), and Bismuth (Bi) in varying concentrations, represents a particularly promising class of these materials.

One of the key advantages of quaternary alloys like GaxIn1-xBiyP1-y is their high degree of tunability. By carefully adjusting the molar fractions 'x' (for Ga) and 'y' (for Bi), it is possible to engineer fundamental material properties such as the band gap energy (Adachi., 2009). This compositional tuning can be performed while simultaneously satisfying the lattice-matching condition to readily available binary substrates, such as Indium Phosphide (InP). Lattice matching is vital for the epitaxial growth of high-quality, low-defect heterostructures, which form the basis of many advanced semiconductor devices (Adachi., 2009). InP is a standard substrate for devices operating in the near-infrared, particularly for telecommunications applications (Zhang et al., 2019),(Wyckoff, 1986), (Meiners, 1986).

The GaxIn1-xBiyP1-y system can be conceptualized as deriving from the binary endpoints GaP, InP, GaBi, and InBi (Adachi, 2009). These binaries exhibit a wide range of lattice constants (from 5.451 Å for GaP (Jain et al., 2022) to 6.628 Å for InBi (Gandouzi et al., 2018) and band gap energies (from 0.00 eV for InBi and GaBi (Wang & Ye, 2002) to 2.35 eV for GaP (Madelung, 2004), with InP at 1.424 eV (Vurgaftman et al., 2001). This wide parameter space theoretically allows GaxIn1-xBiyP1-yalloys to cover a broad spectral range, from the visible to the infrared (0.57–1.72 μm (Paulauskas et al., 2020)), making them attractive candidates for applications including multi-junction solar cells (Adachi., 2009), photodiodes (Jain et al., 2022), infrared lasers (Usman et al., 2019), (Donmez et al., 2021), and heat detectors (Zhang et al., 2019), (Wang et al., 2019), (Paulauskas et al., 2020).

While related ternary alloys like GaInP, GaBiP, InBiP, and InPBi have been subjects of investigation (Kumar et al., 2009) , (Yang et al., 2015), (Samajdar et al., 2016), (Usman et al., 2011), (Wu et al., 2016), (Gelczuk et al., 2016) , (Nattermann et al., 2017) , and successful growth of InPBi has been reported (Wang et al., 2014), theoretical understanding of the quaternary GaxIn1-xBiyP1-y especially under lattice-matched conditions to InP, is essential for realizing its technological potential. (Berding et al., 1988) investigated InPBi theoretically, and GaInP as a basic material for red laser diodes (Meiners, 1986).

This work focuses on a first-principles theoretical investigation of the fundamental structural, electronic, and optical properties of GaxIn1-xBiyP1-y alloys designed to be lattice-matched to an InP substrate, aiming to provide insights for future materials design and device fabrication.

Method

The theoretical investigation was conducted using density functional theory (DFT) (Kohnet al., 1965), (Ceperley et al., 1980), employing the full-potential linearized augmented plane wave (FP-LAPW) method as implemented in the Wien2k computational package (Blaha et al., 2019). This method is known for its high accuracy in calculating the electronic structure and related properties of solids.

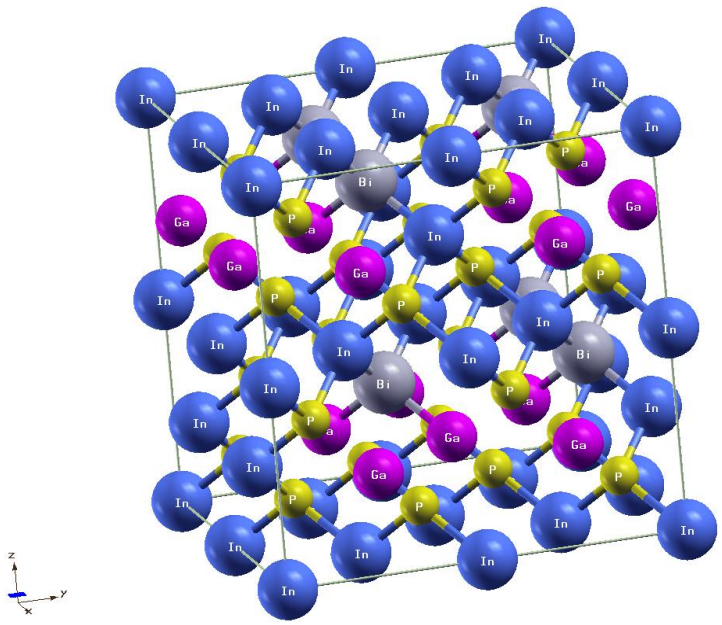

Figure 1. Crystal structure of the 32-atom SQS supercell for $Ga_{0.375}In_{0.625}Bi_{0.1875}P_{0.8125}$ (Q3), representing a lattice-matched $Ga_xIn_{1-x}Bi_yP_{1-y}$ alloy.

To model the GaxIn1-xBiyP1-y quaternary alloys with varying compositions (x, y), we utilized the special quasi-random structure (SQS) approach developed by Zunger (Zunger et al., 1990). This method allows for the modeling of random alloys using relatively small, ordered supercells that mimic the essential correlation functions of the truly random alloy. A 32-atom simple cubic (2×2×2) supercell was constructed for this purpose. An example structure forGa0.375 In 0.625 Bi 0.1875 P0.8125 (Q3) is shown in (Figure 1).

Different exchange-correlation functionals were employed depending on the property being calculated. For structural optimization (determining equilibrium lattice constants and bulk moduli), the local density approximation (LDA) (Kohn et al., 1965), (Ceperley et al., 1980) and the Wu-Cohen generalized gradient approximation (WC-GGA) (Wu et al., 2006)] were used. For electronic and optical properties, the Engel-Vosko GGA (EV-GGA) (Engel et al., 1993) and the Tran-Blaha modified Becke-Johnson potential (TB-mBJ) (Tran et al., 2009) were utilized. The TB-mBJ functional is particularly noted for providing improved band gap predictions compared to standard LDA/GGA functionals. The calculations were performed with the following parameters:

- Plane wave cut-off: RMT * KMAX = 8, where RMT is the smallest muffin-tin radius.
- Maximum angular momentum: IMAX = 10 within the muffin-tin spheres.
- Muffin-tin radii (RMT): Ga = 2.0 a.u., In = 2.1 a.u., Bi = 2.5 a.u., and P = 2.0 a.u. (1 a.u. = 0.52917 Å).
- Energy convergence criterion: 10^{-4} Ry for self-consistent field (SCF) iterations.
- Core-valence state separation: -6 Ryd.
- Brillouin zone integration: A k-point mesh equivalent to 5000 k-points in the full Brillouin zone was used for structural calculations. For optical property calculations, which require denser sampling, 172 k-points in the irreducible Brillouin zone were employed using a methodology suitable for optical properties (Abt et al., 1994) , (Ambrosch-Draxelet al., 2006).

Vegard's law (Adachi., 2009) was used as an initial guide to estimate lattice constants for different compositions (x, y) and to establish the relationship between x and y required for lattice matching to the InP substrate. The lattice constant of the quaternary alloys was then fixed to the calculated value for InP using the WC-GGA functional (5.8908 Å) for subsequent electronic and optical property calculations, simulating perfect epitaxial growth on InP.

Results and Discussion

Structural Properties

First, the structural properties (equilibrium lattice constant 'a' and bulk modulus 'B') of the parent binary compounds (InP, InBi, GaP, GaBi) were calculated using both LDA and WC-GGA. The results are presented in (Table 1) and compared with available experimental and theoretical data (Levinshtein et al., 1996), (Janotti et al., 2002), (Gandouzi et al., 2018), (Wang et al., 2002), (Madelung., 2004), (Vurgaftman et al., 2001), (Liu et al., 2007) , (Assali et al., 2020), (Celin-Manceraet al., 2016) , (Benchehima et al., 2016). The WC-GGA functional generally provides lattice constants closer to experimental values for InP, albeit with a slight overestimation typical of GGA, while LDA tends to underestimate '*a*'. Based on its reasonable agreement for InP (Wyckoff., 1986), (Benchehima et al., 2016), the WC-GGA value for InP (*a* = 5.8908 Å) was chosen as the target lattice constant for the lattice-matched quaternary alloys.

Using Vegard's law , the lattice constant of $Ga_xIn_{1-x}Bi_yP_{1-y}$ can be expressed as:

$$a(x,y) = x(1-y)\cdot a_{GaP} + xy\cdot a_{GaBi} + (1-x)(1-y)\cdot a_{InP} + (1-x)y\cdot a_{InBi} \quad (1)$$

Substituting our calculated WC-GGA binary lattice constants, we get:

$$a(x,y) = -0.4418x + 0.8439y + 0.0611xy + 5.8908\ (\text{Å}) \quad (2)$$

Setting $a(x,y)$ equal to the WC-GGA lattice constant of InP (5.8908 Å) yields the condition for lattice matching:

$$y = 0.4418x/(0.0611x + 0.8439) \text{ for } 0 \leq x \leq 1 \quad (3)$$

This equation defines the specific combinations of (x,y) that result in alloys lattice-matched to InP.

We investigated seven such compositions, denoted Q1 to Q7, corresponding to x = 0.125, 0.250, 0.375, 0.500, 0.625, 0.750, and 0.875, respectively, with corresponding y values determined by Eq. 4 (e.g., Q1: (0.125, 0.0625), Q3: (0.375, 0.1875), Q7: (0.875, 0.4375)). The calculated lattice constants and bulk moduli for these compositions using WC-GGA are included in (Table 1). The lattice constants for these compositions are indeed very close to 5.9 Å, confirming their suitability for lattice-matched growth on InP.

Table 1**.** Calculated lattice constant a, bulk modulus B for binary compounds and selected lattice-matched $Ga_xIn_{1-x}Bi_yP_{1-y}$ quaternary alloys (Q1-Q7, $a \approx 5.8908$ Å) using (LDA)/(WC-GGA), compared with other works.

$Ga_xIn_{1-x}Bi_yP_{1-y}$		**Present work**		**Other Works**			
		(LDA)/(GGA-WC)		**Theoretical**		**Experimental**	
x	*y*	*a* (Å)	B*(*GPa)	*a* (Å)	B*(*GPa)	*a* (Å)	B*(*GPa)
0 (InP)	0	5.8388 [a] 5.8908 [b]	71.5771 [a] 67.0433 [b]	5.830 **[4]** , 5.896 **[9]**,	69.437 **[9]**	5.869 **[2]**	72 **[2]**
0 (InBi)	1	6.6627 [a] 6.7347 [b]	40.7901 [a] 37.7449 [b]	6.628 **[4]**,6.526 **[5]**, 6.80 **[6]**	47.6 **[5]**, 38.3 **[3]**	6.5 **[10]**, 6.626 **[11]**	-
1 (GaP)	0	5.4063 [a] 5.4490 [b]	90.7939 [a] 85.1140 [b]	5.441**[7]**,5.44 **[8]**	84.52 **[7]**, 4.43**[8]**	5.451 **[1]**	88**[1]**
1 GaBi	1	6.2886 [a] 6.3540 [b]	47.3768 [a] 45.3115 [b]	6.178 **[5]** ,6.324**[3]**	46.1 **[5]**, 45.1**[3]**	-	-
0.125	0.0625	5.84965 [a] 5.90175 [b]	69.0690 [a] 64.8858 [b]	-	-	-	-
0. 250	0.125	5.8705 [a] 5.92455 [b]	66.4599 [a] 62.1865 [b]	-	-	-	-
0.375	0.1875	5.8873 [a] 5.9425 [b]	64.2428 [a] 60.259 [b]	-	-	-	-
0.500	0.250	5.89605 [a] 5.94955	62.7793 [a] 59.1181 [b]	-	-	-	-
0.625	0.3125	5.90515 [a] 5.96095 [b]	61.6372 [a] 57.8936 [b]	-	-	-	-
0.750	0.375	5.9043 [a] 5.9609 [b]	60.7463 [a] 57.3657 [b]	-	-	-	-
0.875	0.4375	5.9035 [a] 5.9610 [b]	59.8525 [a] 56.5951 [b]	-	-	-	-

[a] *calculated from LDA scheme,* [b] *calculated from WC-GGA scheme.*

[1] (Levinshtein et al., 1996) **[2]** (Wyckoff, 1986) **[3]** (Janotti et al., 2002)
[4] (Gandouzi et al., 2018) **[5]** (Wang et al., 2002) **[6]** (Liu et al., 2007)
[7] (Assali et al., 2020) **[8]** (Celin-Mancera et al., 2016) **[9]** (Benchehima et al., 2016)
[10] (Okamoto and K. Oe., 1998) **[11]** (Rajpalke et al., 2014)

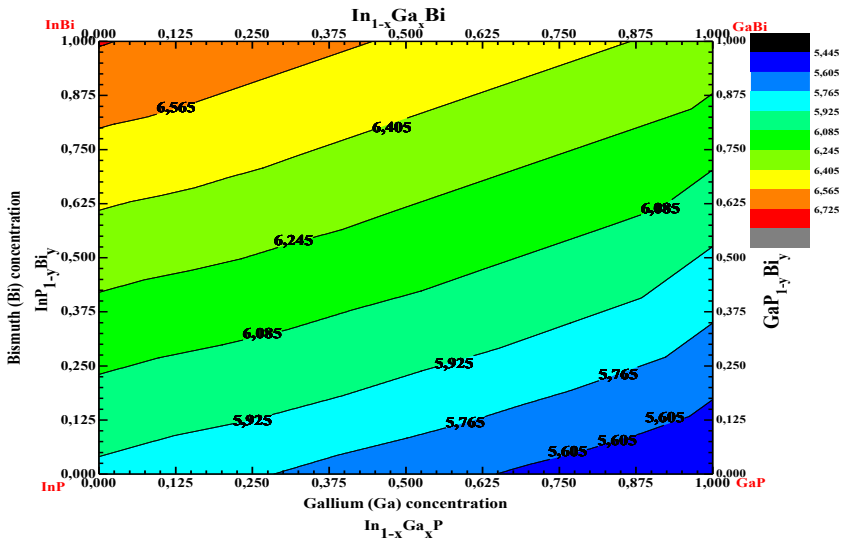

Figure 2. Contour map of the calculated lattice constant a (WC-GGA, in Å) for $Ga_xIn_{1-x}Bi_yP_{1-y}$ as a function of Ga (x) and Bi (y) concentrations.

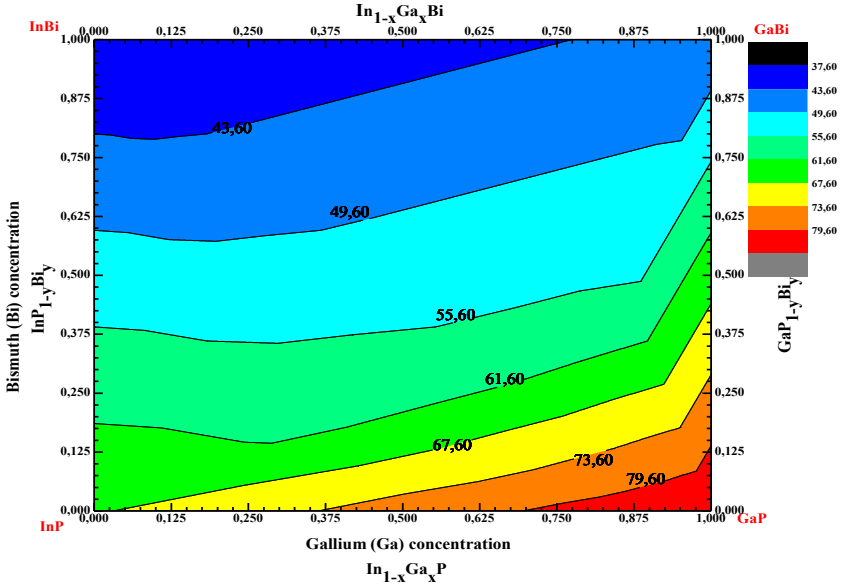

Figure 3. Contour map of the calculated bulk modulus B (WC-GGA, in GPa) for $Ga_xIn_{1-x}Bi_yP_{1-y}$ as a function of Ga (x) and Bi (y) concentrations

Figure 2 illustrates the variation of the lattice constant across the composition range, consistent with Vegard's law. Figure 3 shows the variation of the bulk modulus.

Electronic Properties

The electronic band structures and density of states (DOS) were calculated for the lattice-matched compositions Q1-Q7 using the EV-GGA (Engel et al., 1993) and TB-mBJ(Tran et al., 2009)potentials, with the lattice constant fixed at the InP WC-GGA value (5.8908 Å). The TB-mBJ potential generally yields band gaps in better agreement with experimental values for III-V semiconductors.

Table 2 shows the calculated TB-mBJ band gaps (Eg). Our values for the binaries InP (1.560 eV) and GaP (2.255 eV) agree well with experimental data (Madelung., 2004),(Vurgaftman et al., 2001) and previous calculations (Gandouzi et al., 2018), (Celin-Mancera et al., 2016),(Jiang et al., 2013), (Camargo-Martínez et al., 2012). The calculated band gaps for GaBi and InBi are 0.00 eV, consistent with their semi-metallic or narrow-gap nature reported previously (Wang et al., 2002), (Figs. 4 and 5).

Table 2. Calculated band gap energies Eg (in eV) using EV-GGA and TB-mBJ potentials for binary compounds and the lattice-matched $Ga_xIn_{1-x}Bi_yP_{1-y}$ quaternary alloys (Q1-Q7). Comparison with other works.

	$Ga_xIn_{1-x}Bi_yP_{1-y}$		**Present work**		**Other works**	
	x	***y***	**EV-GGA**	**TB-mBJ**	**TB-mBJ**	**Experimental**
InP	0 (InP)	0	1.237	1.560	1.41 **[5]**,1.680 **[1]**	1.424 **[4]**
InBi	0 (InBi)	1	-0.031	0.000	0.000 **[2]**	-
GaP	1 GaP	0	2.233	2.255	2.24 **[7]**, 2.30 **[6]**	2.35 **[3]**
GaBi	1 GaBi	1	-0.046	0.000	0.000 **[2]**	-
Q1	$Ga_{0.125}In_{0.875}Bi_{0.0625}P_{0.9375}$		0.994	1.360	-	-
Q2	$Ga_{0.250}In_{0.750}Bi_{0.125}P_{0.875}$		0.749	1.147	-	-
Q3	$Ga_{0.375}In_{0.625}Bi_{0.1875}P_{0.8125}$		0.563	0.994	-	-
Q4	$Ga_{0.500}In_{0.500}Bi_{0.250}P_{0.750}$		0.400	0.855	-	-
Q5	$Ga_{0.625}In_{0.375}Bi_{0.3125}P_{0.6875}$		0.227	0.707	-	-
Q6	$Ga_{0.750}In_{0.250}Bi_{0.375}P_{0.625}$		0.105	0.606	-	-
Q7	$Ga_{0.875}In_{0.125}Bi_{0.4375}P_{0.5625}$		0.021	0.503	-	-

[1] (Gandouzi et al., 2018) **[2]** (Wang et al., 2002) **[3]** (Madelung., 2004) **[4]** (Vurgaftman et al., 2001)
[5] (Gazhulina et al., 2015) **[6]** (Jiang , 2013) **[7]** (Camargo-Martínez et al., 2012)

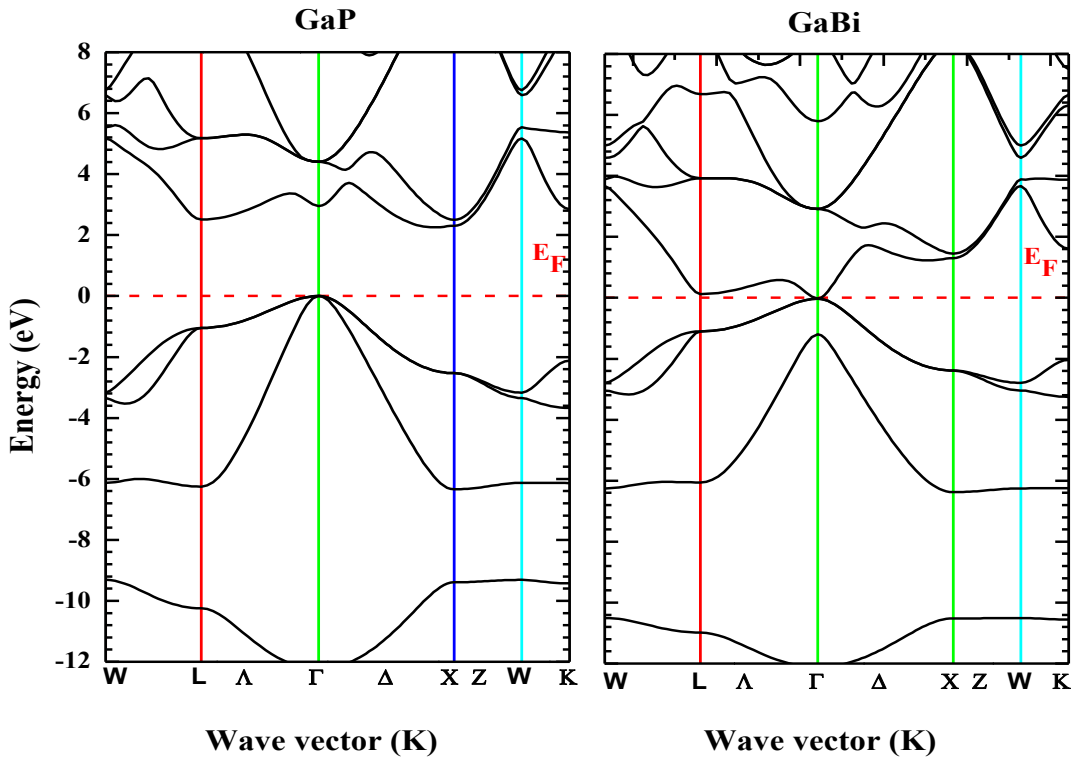

Figure 4. Electronic band structure of GaP (indirect) and GaBi (direct) binaries along high symmetry directions, calculated using TB-mBJ. Fermi level (EF) is at 0 eV.

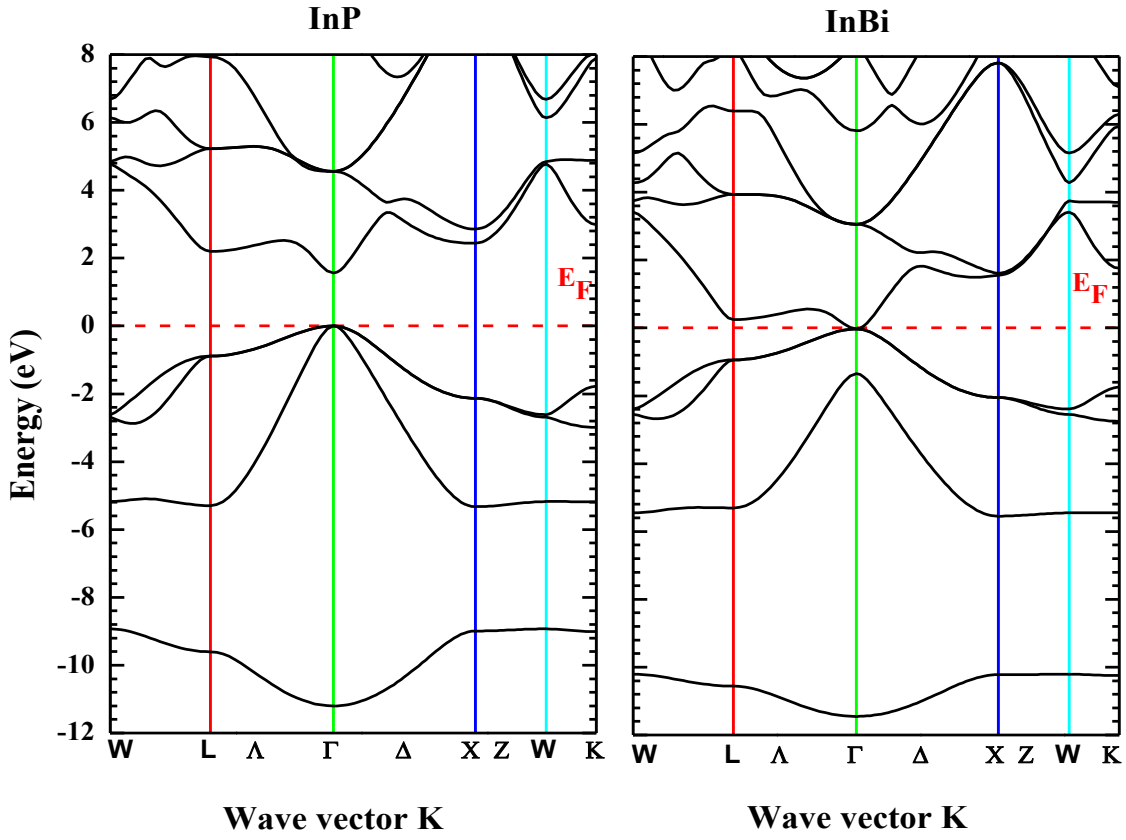

Figure 5. Electronic band structure of InP (direct) and InBi (direct) binaries along high symmetry directions, calculated using TB-mBJ. Fermi level (EF) is at 0 eV

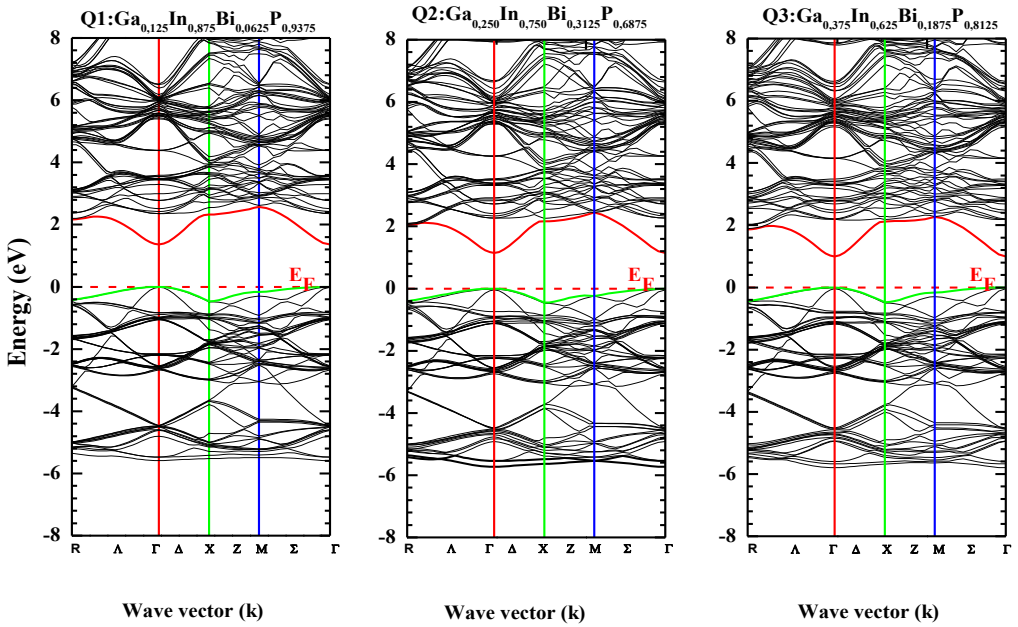

Figure 6. Electronic band structures of lattice-matched $Ga_xIn_{1-x}Bi_yP_{1-y}$ alloys for compositions Q1, Q2, and Q3 along high symmetry directions, calculated using TB-mBJ. The Fermi level (EF) is set to 0 eV.

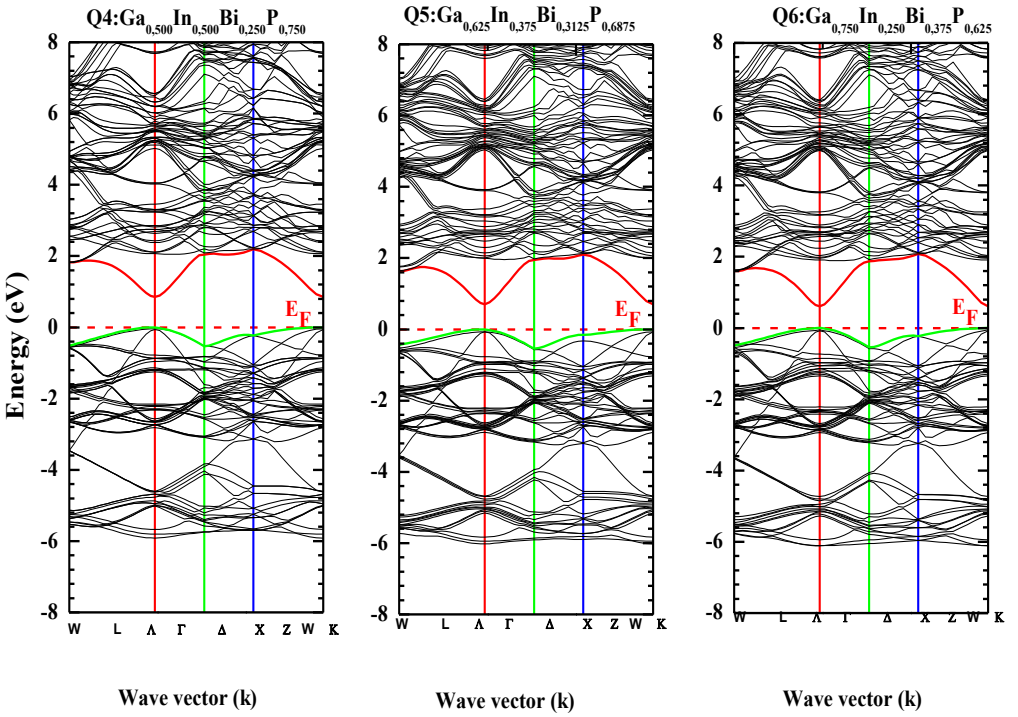

Figure 7. Electronic band structures of lattice-matched GaxIn1-xBiyP1-y alloys for compositions Q4, Q5, and Q6 along high symmetry directions, calculated using TB-mBJ. The Fermi level (EF) is set to 0 eV.

The calculated band structures for compositions Q1-Q7 (Figs. 6 and 7) clearly demonstrate that all these lattice-matched $Ga_xIn_{1-x}Bi_yP_{1-y}$ alloys possess a direct band gap at the Γ point (center of the Brillouin zone). This is consistent with the binary constituents except GaP (Madelung., 2004) and is highly desirable for optoelectronic applications like lasers and efficient light emitters/absorbers.

Figure 8 presents a contour map of the TB-mBJ calculated band gap. Along the lattice-matching line (Eq. 3), the band gap energy decreases significantly as both *x* and *y* increase. The calculated electronic band gap ranges from 1.360 eV (for Q1, *x*=0.125, *y*=0.0625) down to 0.503 eV (for Q7, *x*=0.875, *y*=0.4375). This tunable band gap corresponds to wavelengths ranging from approximately 0.911 µm to 2.456 µm. This range effectively covers the important telecommunication wavelengths of 1.3 µm and 1.55 µm.

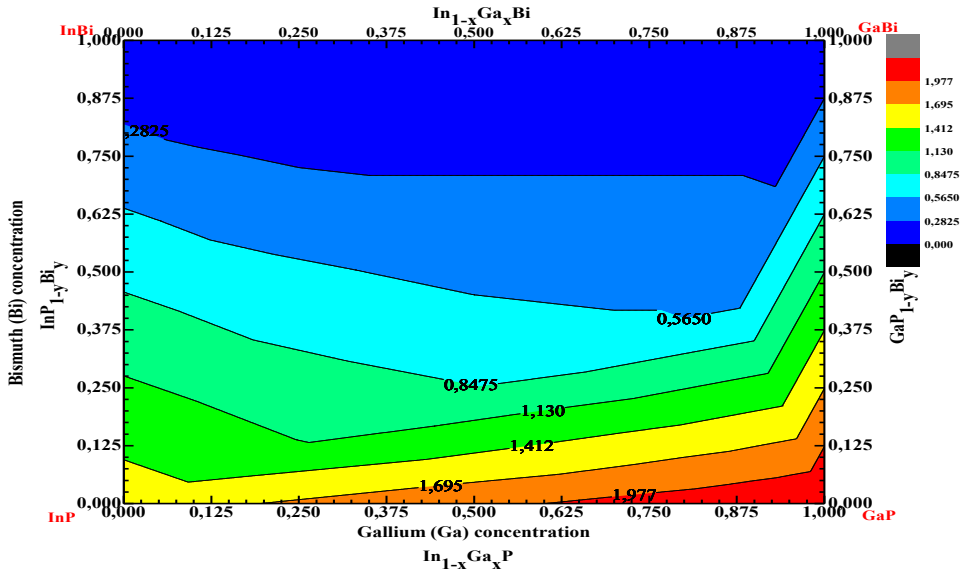

Figure 8. Contour map of the calculated direct band gap energy Eg (TB-mBJ, in eV) for $Ga_xIn_{1-x}Bi_yP_{1-y}$as a function of Ga (x) and Bi (y) concentrations.

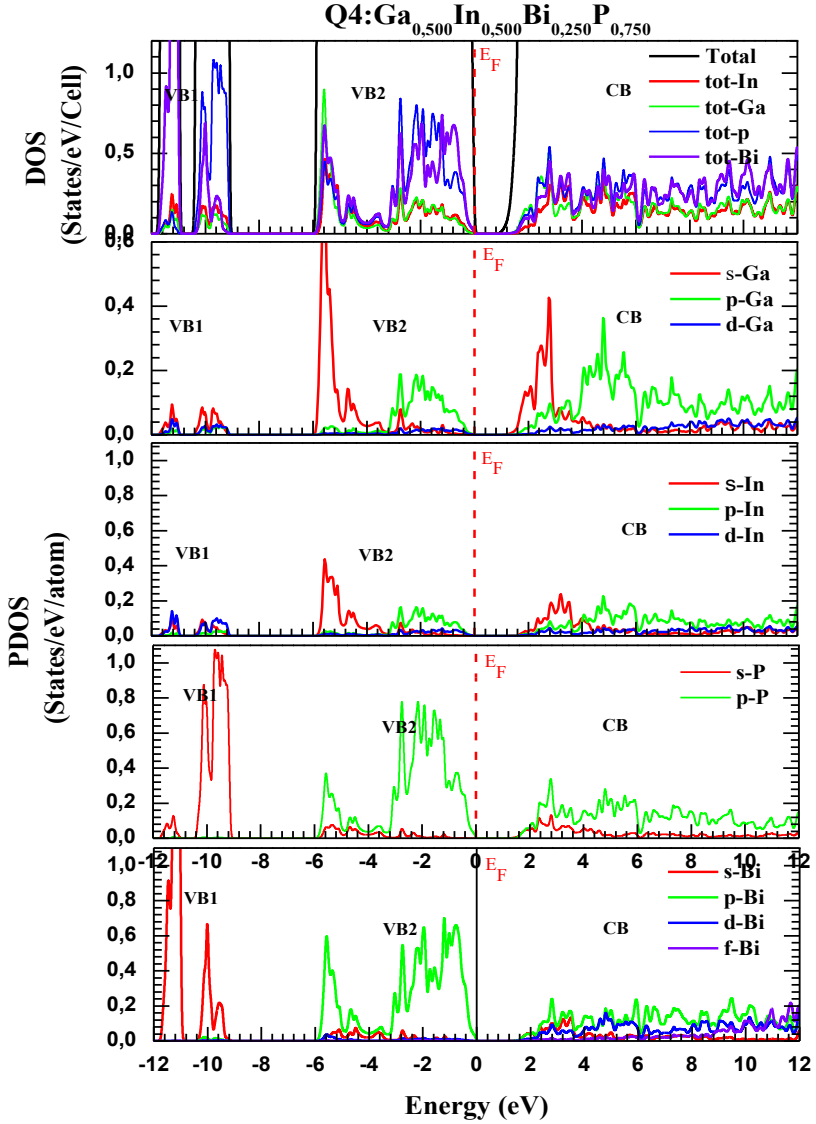

Figure 9.Total and partial density of states (TDOS/PDOS) for the lattice-matched quaternary alloy Q4 ($Ga_{0.500}In_{0.500}Bi_{0.250}P_{0.750}$), calculated using TB-mBJ. EF is at 0 eV.

The total and partial density of states (TDOS/PDOS) provides further insight. (Figure 9) shows the DOS for composition Q4 as an example. The valence band (VB) consists of regions dominated by Bi-s, P-s states at lower energy (VB_0, ~-11.5 to -8.9 eV), hybridization of Ga-s, In-s, P-p states (VB_1, ~-5.6 to -3.6 eV), and primarily Bi-p, P-p states near the VBM (VB_2, ~-3.6 eV to EF). (CB) region is formed by mixture of (s, p) states of (Bi- Ga- In- P) atoms, d states of (Bi- Ga- In) atoms and f states of Bi atom. The conduction band minimum (CBMin) is mainly formed by s states of Bi, Ga, and P atoms. The incorporation of Bi significantly influences the position of both the valence band maximum (VBM) and the CBMin, leading to the observed band gap reduction.

Optical Properties

The optical properties of the lattice-matched $Ga_xIn_{1-x}Bi_yP_{1-y}$ alloys (Q1-Q7) and their binary constituents were calculated using the TB-mBJ potential (Tran et al., 2009).

Complex Dielectric Function ε(ω)

The complex dielectric function $\varepsilon(\omega) = \varepsilon_1(\omega) + i\varepsilon_2(\omega)$is fundamental for describing optical response (Adachi, 2009). $\varepsilon_2(\omega)$ is calculated directly from electronic structure, and $\varepsilon_1(\omega)$ is obtained via the Kramers-Kronig relation (Adachi, 2009), (Slimani et al., 2019) , (Bouragba et al., 2020).

$$\varepsilon_2(\omega) = \left(\frac{4\pi^2 e^2}{m^2\omega^2}\right)\sum_{ij}\int\langle i|M|j\rangle^2 f_i\,(1-f_i)\delta(E_f - E_i - \omega)\mathrm{d}^3k, \qquad (4)$$

$$\varepsilon_1(\omega) = 1 + \frac{2}{\pi}\mathrm{p}\int_0^{\infty}\frac{\omega'.\varepsilon_2(\omega')}{\omega'^2-\omega^2}d\omega' \ , \qquad (5)$$

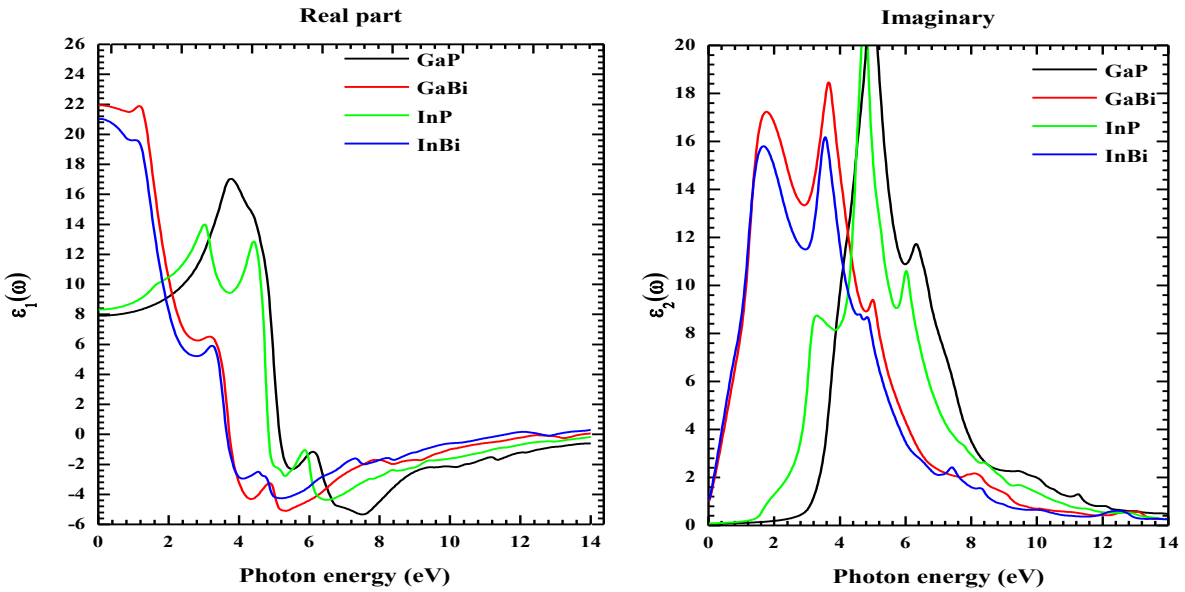

Figure 10. Calculated real (ε_1) and imaginary (ε_2) parts of the complex dielectric function for the binary compounds InP, InBi, GaP, GaBi, using the TB-mBJ scheme.

The calculated dielectric functions for the binaries (Figure 10) are consistent with known features. For the quaternaries (Figures 11, 12), the static dielectric constant $\varepsilon_1(0)$ (Table 3) increases as *x* and *y* increase (i.e., from Q1 to Q7), which is consistent with the Penn model (Penn, 1962) where $\varepsilon_1(0)$ is inversely related to the square of the band gap (Eg). The imaginary part $\varepsilon_2(\omega)$ shows critical points (peaks denoted E_0, E_1, E_2, E_3 in Table 3) associated with direct electronic transitions between VB and CB states. The first critical point E_0 corresponds to the fundamental absorption edge (the band gap Eg). As seen in (Table 3), E_0 (derived from $\varepsilon_2(\omega)$ peaks) decreases steadily from Q1 to Q7, following the trend of the calculated band gaps (Table 2).

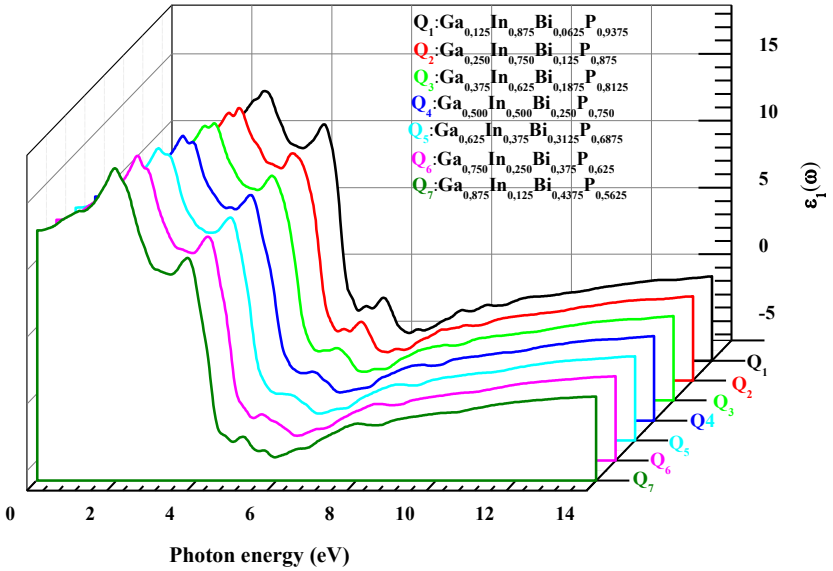

Figure 11. Real part (ε_1) of the dielectric function for the lattice-matched $Ga_xIn_{1-x}Bi_yP_{1-y}$ (Q1-Q7) as a function of photon energy, calculated using TB-mBJ.

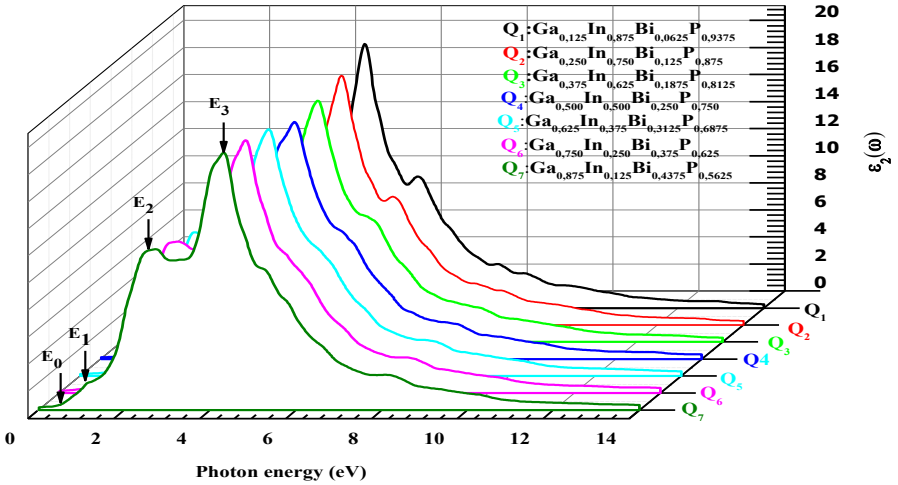

Figure 12. Imaginary part (ε_2) of the dielectric function for the lattice-matched $Ga_xIn_{1-x}Bi_yP_{1-y}$ (Q1-Q7) as a function of photon energy, calculated using TB-mBJ.

Table 3. Calculated critical point energies (E_0, E_1, E_2, E_3 in eV) from $\varepsilon_2(\omega)$ spectra and the static dielectric constant $\varepsilon_1(0)$ for binaries and lattice-matched $Ga_xIn_{1-x}Bi_yP_{1-y}$ alloys (Q1-Q7), using TB-mBJ.

$Ga_xIn_{1-x}Bi_yP_{1-y}$	Present work					Other works				
x	**E_0**	**E_1**	**E_2**	**E_3**	**$\varepsilon_1(0)$**	**E_0**	**E_1**	**E_2**	**E_3**	**$\varepsilon_1(0)$**
0 (InP)	1.56	1.825	3.246	4.76	8,320	1.570 **[1]**	-	3.284 **[1]**	4.760**[1]**	8.318 **[1]**
0 (InBi)	0.00	1.675	3.551	4.623	21,019	-	-	-	-	-
1 (GaBi	0.00	1.734	3.643	5.18	21,940	-	-	-	-	-
1 GaP	2.255	2.421	3.646	4.973	7,908	2.245 **[2]**	-	3.980 **[2]**	5.041 **[2]**	8.024 **[2]**
0.125	1.541	1.836	3.327	4.702	8.763	-	-	-	-	-
0. 250	1.125	1.649	2.247	4.622	9.267	-	-	-	-	-
0.375	0.997	1.544	3.094	4.567	9.796	-	-	-	-	-
0.500	0.663	1.381	2.698	4.516	10.296	-	-	-	-	-
0.625	0.635	1.264	2.616	4.376	10.965	-	-	-	-	-
0.750	0.508	1.229	2.547	4.341	11.547	-	-	-	-	-
0.875	0.301	1.125	2.477	4.294	12.246	-	-	-	-	-

[1] (Benchehima et al., 2016) **[2]** (Hachemi et al., 2022)

Complex Refractive Index

The refractive index $n(\omega)$ and extinction coefficient $k(\omega)$ are derived from $\varepsilon(\omega)$ (Adachi, 2009), (Benchehima et al., 2017), (Benchehima et al., 2018) :

$$n(\omega) = \sqrt{\frac{(\varepsilon_1^2(\omega)+\varepsilon_2^2(\omega))^{1/2}+\varepsilon_1(\omega)}{2}} \quad (6)$$

$$k(\omega) = \sqrt{\frac{(\varepsilon_1^2(\omega)^2+\varepsilon_2^2(\omega)^2)^{1/2}-\varepsilon_1(\omega)}{2}} \quad (7)$$

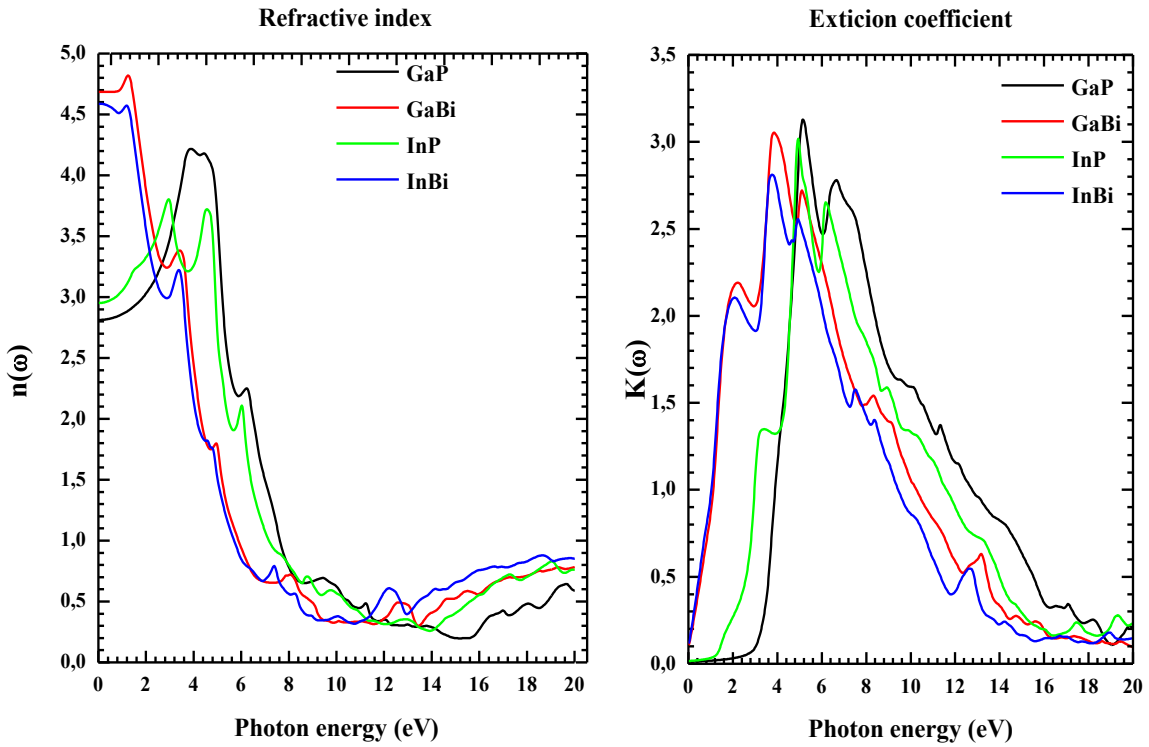

Figure 13. Calculated refractive index $n(\omega)$ and extinction coefficient $k(\omega)$ for binary compounds, using TB-mBJ.

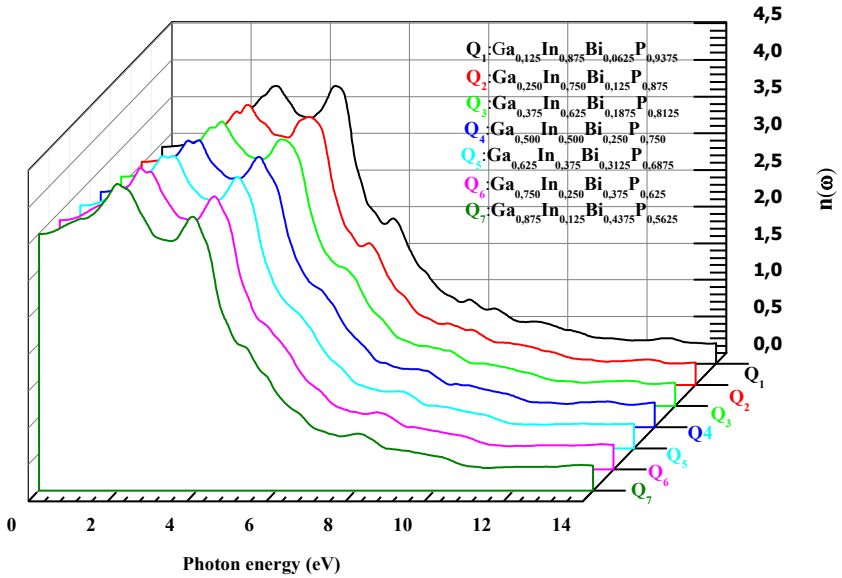

Figure 14. Refractive index $n(\omega)$ for the lattice-matched $Ga_xIn_{1-x}Bi_yP_{1-y}$ alloys (Q1-Q7), calculated using TB-mBJ.

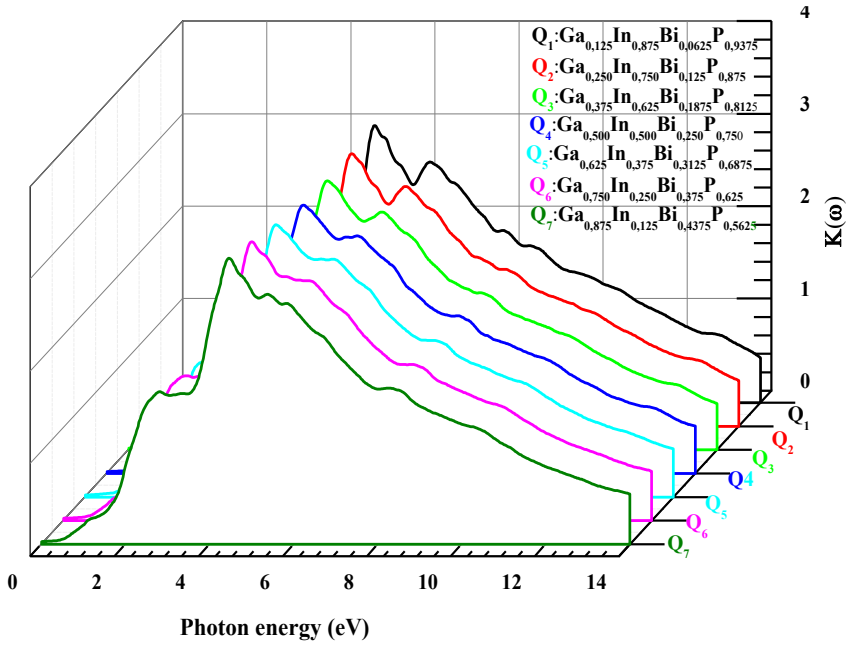

Figure 15. Extinction coefficient $k(\omega)$ for the lattice-matched $Ga_xIn_{1-x}Bi_yP_{1-y}$ alloys (Q1-Q7), calculated using TB-mBJ.

(Figures 13-15) show n(ω) and k(ω). The static refractive index $n(0) = \sqrt{\varepsilon_1(0)}$ (Table 4) also increases with increasing x and y content (from Q1 to Q7), consistent with the trend in $\varepsilon_1(0)$ and the decreasing band gap. The calculated $n(0)$ values for InP and GaP are in good agreement with experimental(Asadi et al., 2019) and other theoretical results (Benchehima et al., 2016), (Hachemi et al., 2022) , (Asadi et al., 2019), (Ahuja et al., 1997). The spectra show characteristic peaks related to the critical points in the electronic structure.

Table 4. Calculated static refractive index $n(0)$ for binaries and lattice-matched $Ga_xIn_{1-x}Bi_yP_{1-y}$ alloys (Q1-Q7), compared with other work.

Compound		***n*(0) refractive index**		
		Present work	**Others work**	
$Ga_xIn_{1-x}Bi_yP_{1-y}$		**TB-mBJ**	**Theoretical**	**Experimental**
x	***y***			
0 (inp)	0	2.884	2.884 **[1]**, 2.81 **[5]**	2.70 **[3]**
0 (InBi)	1	4.586	-	-
1 (GaP	0	2.812	2.832 **[2]**, 2.83 **[4]**	-
1 GaBi	1	4.685	-	-
0.125	0.0625	2.960	-	-
0, 250	0.125	3.044	-	
0.375	0.1875	3.129	-	
0.500	0.250	3.208	-	-
0.625	0.3125	3.311	-	-
0.750	0.375	3.398	-	
0.875	0.4375	3.499	-	

[1] (Benchehima et al., 2016) **[2]** (Hachemi et al., 2022) **[3]** (. Meiners, 2022)
[4] (Asadi et al., 2019) **[5]** (Asadi et al., 1997)

Optical Conductivity and Absorption Coefficient

Optical conductivity σ(ω) and absorption coefficient α(ω) are related to ε(ω) and $k(\omega)$ (Adachi., 2009):

$$\sigma(\omega) = \frac{i\omega}{4\pi}\varepsilon(\omega) \quad (8)$$

$$\alpha(\omega) = \frac{4\pi}{\lambda}k(\omega) \quad (9)$$

where λ is the wavelength in vacuum.

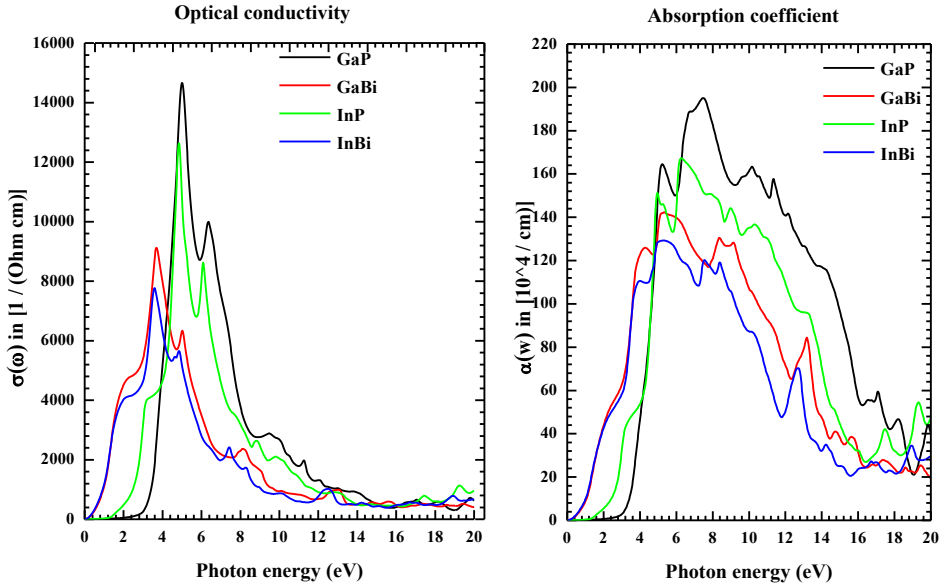

Figure 16. Calculated optical conductivity σ(ω) and absorption coefficient α(ω) for binary compounds, using TB-mBJ.

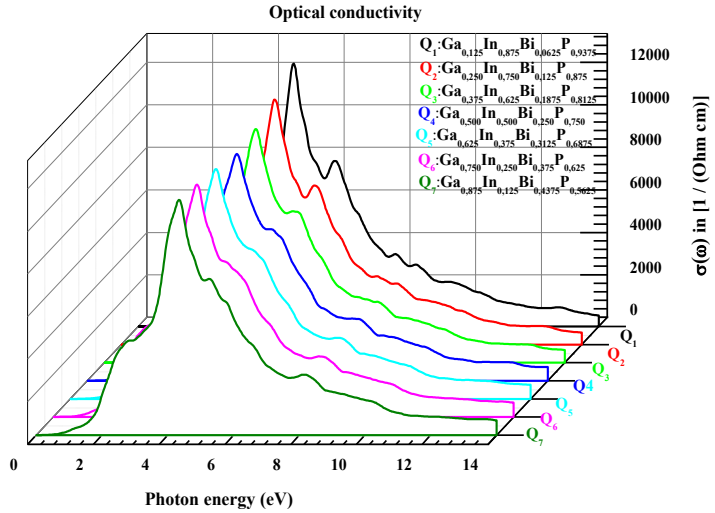

Figure 17.Optical conductivity σ(ω) for the lattice-matched $Ga_xIn_{1-x}Bi_\gamma P_{1-\gamma}$ alloys (Q1-Q7), calculated using TB-mBJ.

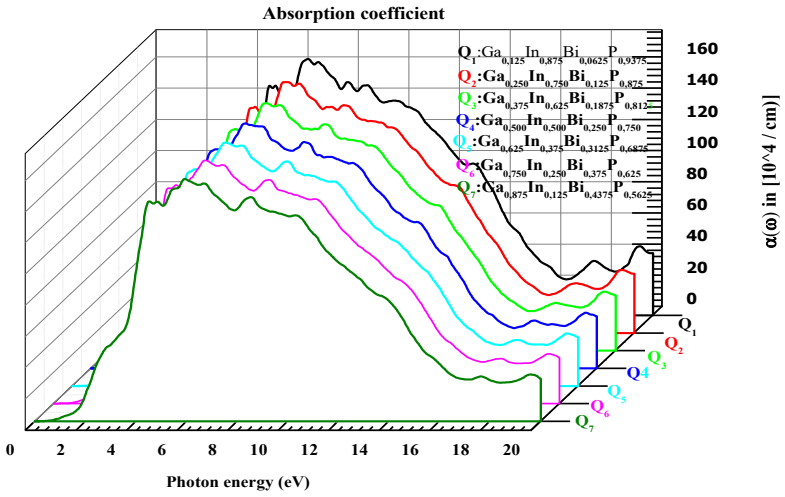

Figure 18. Absorption coefficient α(ω) for the lattice-matched $Ga_xIn_{1-x}Bi_\gamma P_{1-\gamma}$ alloys (Q1-Q7), calculated using TB-mBJ.

The optical conductivity and absorption coefficient are presented in (Figures 16-18). The onset of absorption corresponds to the fundamental band gap Eg (or E_0). For the quaternary alloys, the absorption edge shifts to lower energies as *x* and *y* increase, reflecting the decreasing band gap. The maximum absorption peaks for the quaternaries occur around 6.02 ± 0.6 eV, shifting slightly to lower energies and decreasing in intensity as *x* and *y* increase. The quaternaries show strong absorption in the visible and near-infrared regions (above ~2 eV).

Optical Band Gap

To quantify the optical band gap , Tauc plots were constructed(Tauc et al., 1966), (Rahimi et al., 2022) assuming that the energy-dependent absorption coefficient $\alpha(\omega)$ can be expressed by the following relationship

$$\alpha(\omega)h\nu = B\left(h\nu - E_g^{op}\right)^{n} \quad (10)$$

Where B is a constant for a direct transition, $h\nu$ is the photon's energy, E_g^{op} is the optical band gap and α is the optical absorption coefficient and n refers to an index ($n = ½$ for direct gap or n=2 for indirect gap).

The optical band gap is obtained by extrapolating the linear portion of the $(\alpha h\nu)^2$ and $(h\nu)$plot to the value $(\alpha h\nu)^2 = 0$.

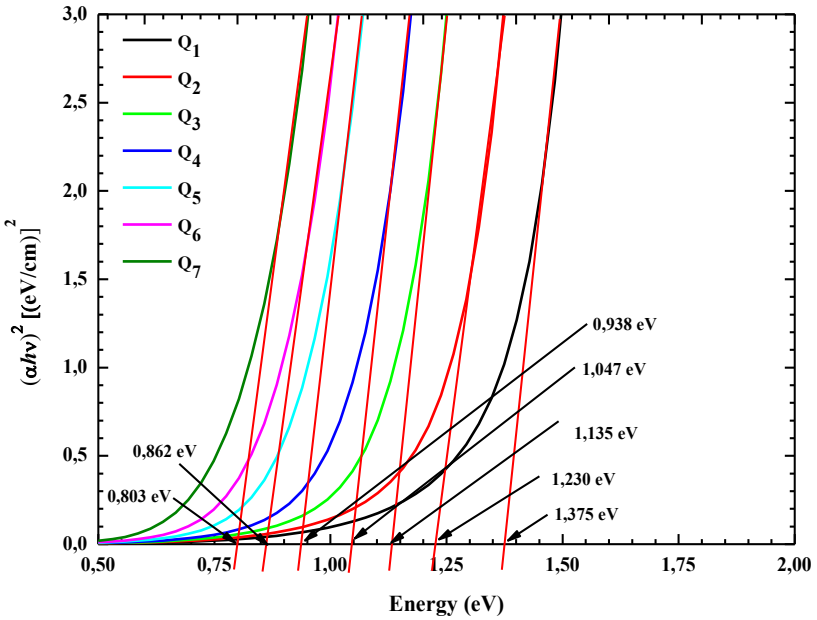

Figure 19.Tauc plots (αhν)² vs. photon energy (hν) for determining the direct optical band gap of lattice-matched $Ga_xIn_{1-x}Bi_yP_{1-y}$ alloys (Q1-Q7), based on TB-mBJ calculations.

Figure 19 shows the Tauc plots for the lattice-matched quaternary compositions. The determined direct optical band gaps are 1.375, 1.230, 1.135, 1.047, 0.938, 0.862, and 0.803 eV for Q1 through Q7, respectively. These values confirm the trend of decreasing band gap with increasing Ga and Bi concentration along the lattice-matching line, consistent with the electronic band gap calculations (Table 2) and E_0 values from $\varepsilon_2(\omega)$ (Table 3). This tunable optical gap covers the wavelength range from ~0.9 µm (for Q1) to ~1.56 µm (for Q7), again highlighting the relevance for telecommunications.

Conclusion

This theoretical study, based on first-principles DFT calculations using the FP-LAPW method (Blaha et al., 2019), has investigated the structural, electronic, and optical properties of $GaxIn_{1-x}Bi_yP_{1-y}$quaternary alloys specifically designed to be lattice-matched to InP substrates. Key findings include:

- The WC-GGA functional (Wu et al., 2006) accurately predicts lattice constants. Compositions satisfying the derived lattice-matching condition (Eq. 3) exhibit lattice parameters close to that of InP (~5.9 Å) based on WC-GGA calculations (Table 1), suitable for epitaxial growth.

- All investigated lattice-matched $Ga_xIn_{1-x}Bi_yP_{1-y}$ alloys possess a direct band gap at the Γ point (Figs. 6, 7). The band gap energy (calculated via TB-mBJ(Blaha et al., 2019)) is highly tunable by adjusting the Ga (x) and Bi (y) fractions along the lattice-matching constraint, ranging from 1.360 eV (Q1) down to 0.503 eV (Q7) (Table 2). This corresponds to a wavelength range of 0.91 µm to 2.46 µm.

- The optical constants (dielectric function, refractive index, absorption coefficient) were calculated using the TB-mBJ scheme (Figs. 10-18). The fundamental absorption edge shifts to lower energies with increasing x and y, consistent with the electronic band gap trend. Tauc analysis (Tauc et al., 1966), (Rahimi et al., 2022) yielded direct optical band gaps decreasing from 1.375 eV (Q1) to 0.796 eV (Q7) (Fig. 19), corresponding to wavelengths from ~0.9 µm to ~1.56 µm.

- The results demonstrate that $Ga_xIn_{1-x}Bi_yP_{1-y}$ alloys lattice-matched to InP offer significant flexibility in tuning the optoelectronic response. The ability to achieve direct band gaps spanning near-infrared wavelengths (~0.9 µm to ~2.5 µm based on electronic gap calculations) while maintaining lattice matching makes this material system highly attractive for optoelectronic device applications. It is particularly promising for lasers and photo detectors operating in the 1.3 µm and 1.55 µm telecommunication windows. This theoretical work provides valuable data and insights for the future development and optimization of $Ga_xIn_{1-x}Bi_yP_{1-y}$/InP based devices.

Scientific Ethics Declaration

* The authors declares that the scientific ethical and legal responsibility of this article published in EPSTEM journal belongs to the authors.

Conflict of Interest

* The authors declare that they have no conflicts of interest

Funding

* This research received no specific grant from any funding agency in the public, commercial, or not-for-profit sectors.

Acknowledgements or Notes

* This article was presented as a poster presentation at the International Conference on Technology, Engineering and Science (www.icontes.net) held in Antalya/Türkiye on November 12-15, 2025.

* The authors express gratitude to the Djillali Liabes University of Sidi Bel Abbes .

* The authors would like to thank the conference committee and the referees who reviewed the article for their valuable feedback.

References

Abt, R., Ambrosch-Draxl, C., & Knoll, P. (1994). Optical response of high temperature superconductors by full potential LAPW band structure calculations. *Physica B: Condensed Matter, 194–196*, 1451–1452.

Adachi, S. (2009). *Properties of semiconductor alloys: Group-IV, III-V and II-VI semiconductors*. John Wiley & Sons.

Ahuja, R., Auluck, S., Eriksson, O., Wills, J. M., & Johansson, B. (1997). Electronic and optical properties of InP. *Solid State Communications, 104*(5), 249–252.

Ambrosch-Draxl, C., & Sofo, J. O. (2006). Linear optical properties of solids within the full-potential linearized augmented plane wave method. *Computer Physics Communications, 175*(1), 1–14.

Asadi, Y., & Nourbakhsh, Z. (2019). Study of the linear and nonlinear response properties of the zinc-blende AlP, GaP and their AlxGa1-xP ternary alloys using first principle calculations. *Computational Condensed Matter, 21*, e00410.

Assali, A., Kanouni, F., Zou, Q., & Khenata, R. (2020). Optical characteristics of dilute gallium phosphide bismide: Promising material for near-infra photonic device applications. *Physics Letters A, 384*(5), 126147.

Benchehima, M., & Abid, H. (2016). Electronic and optical properties of AlxGayIn1-x–yAs quaternary alloys with and without relaxation lattice matched to InP for laser applications: First-principles study. *Optik, 127*(16), 6541–6558.

Benchehima, M., Abid, H., & Benchikh, K. (2017). First-principles calculations of the structural and optoelectronic properties of BSb1-xAsx ternary alloys in zinc blende structure. *Materials Chemistry and Physics, 198*, 214-228.

Benchehima, M., Abid, H., Sadoun, A., & Chaouche, A. C. (2018). The electrical properties of Au/GaN and PEDOT: PSS/GaN diodes. *Computational Materials Science, 155*, 224-234.

Berding, M. A., Sher, A., Chen, A. B., & Miller, W. (1988). Structural properties of bismuth-bearing semiconductor alloys. *Journal of Applied Physics, 63*(1), 107-115.

Blaha, P., Schwarz, K., Madsen, G. K. H., Kvasnicka, D., Luitz, J., Laskowski, R., Tran, F., & Marks, L. D. (2019). *WIEN2k: An augmented plane wave plus local orbitals program for calculating crystal properties* (Computer software). Technische Universität Wien.

Bouragba, D., Benchehima, M., Abid, H., & Djili, A. (2020). Optical response functions and thermodynamic stability of BSb1-xNx ternary alloys in zinc blende structure. *Optik, 222*, 165472.

Camargo-Martínez, J. A., & Baquero, R. (2012). Performance of the modified Becke-Johnson potential for semiconductors. *Physical Review B, 86*(19), 195106.

Celin-Mancera, W. A., López-Pérez, W., González-García, Á., Ramírez-Montes, L., & González-Hernández, R. (2016). Theoretical study of structural stability, elastic, electronic and thermodynamic properties of ScxGa1-xP compounds by ab initio calculations. *Computational Condensed Matter, 8*, 14–21.

Ceperley, D. M., & Alder, B. J. (1980). Ground state of the electron gas by a stochastic method. *Physical Review Letters, 45*(7), 566–569.

Donmez, O., Erol, A., Çetinkaya, Ç., Çokduygulular, E., Aydın, M., Yıldırım, S., & Gunes, M. (2021). A quantitative analysis of electronic transport in n-and p-type modulation-doped GaAsBi/AlGaAs quantum well structures. *Semiconductor Science and Technology, 36*(11), 115017.

Engel, E., & Vosko, S. H. (1993). Exact exchange-only potentials and the virial relation as microscopic criteria for generalized gradient approximations. *Physical Review B, 47*(20), 13164.

Gandouzi, M., Hedhili, F., & Rekik, N. (2018). A density functional theory investigation of the structural and optoelectronic properties of InP1-xBix alloys. *Computational Materials Science, 149*, 307-315.

Gazhulina, A. P., & Marychev, M. O. (2015). Structural, electronic and nonlinear optical properties of B3 and B20 compounds: A first-principles investigation within the LDA, GGA and modified Becke-Johnson exchange potential plus LDA. *Journal of Alloys and Compounds, 623*, 413–437.

Gelczuk, Ł., Stokowski, H., Kopaczek, J., Zhang, L., Li, Y., Wang, K., & Kudrawiec, R. (2016). Bi-induced acceptor level responsible for partial compensation of native free electron density in InP1-xBix dilute bismide alloys. *Journal of Physics D: Applied Physics, 49*(11), 115107.

Hachemi, M. H., Benchehima, M., Bencherif, K., & Abid, H. (2022). The effect of N-incorporation on the structural and optoelectronic properties of GaP and GaAs for optical telecommunication applications: First-principles study. *Optik, 262*, 169282.

Jain, N., Mal, I., Samajdar, D., & Bagga, N. (2022). Investigation of optoelectronic performance of InAsNBi for infrared detection. In *Tailored functional materials* (pp. 475–484). Springer.

Janotti, A., Wei, S.-H., & Zhang, S. (2002). Theoretical study of the effects of isovalent coalloying of Bi and N in GaAs. *Physical Review B, 65*(11), 115203.

Jiang, H. (2013). Band gaps from the Tran-Blaha modified Becke-Johnson approach: A systematic investigation. *The Journal of Chemical Physics, 138*(13), 134115.

Kohn, W., & Sham, L. J. (1965). Self-consistent equations including exchange and correlation effects. *Physical Review, 140*(4A), A1133.

Kumar, S., Parashari, S. S., & Auluck, S. (2009). Disorder effects on electronic and optical properties of the ternary GaxIn1-xP (x=0.25, 0.50, and 0.75) alloy. *Physica Status Solidi (b), 246*(10), 2294-2300.

Levinshtein, M., Rumyantsev, S., & Shur, M. (1996). *Handbook series on semiconductor parameters: Volume 1: Si, Ge, C (Diamond), GaAs, GaP, GaSb, InAs, InP, InSb*. World Scientific.

Liu, W., Zheng, W. T., & Jiang, Q. (2007). First-principles study of the surface energy and work function of III-V semiconductor compounds. *Physical Review B, 75*(23), 235322.

Madelung, O. (2004). III-V compounds. In *Semiconductors: Data handbook* (pp. 71–172). Springer.

Meiners, L. G. (1986). Temperature dependence of the dielectric constant of InP. *Journal of Applied Physics, 59*(5), 1611–1613.

Murnaghan, F. D. (1944). The compressibility of media under extreme pressures. *Proceedings of the National Academy of Sciences of the United States of America, 30*(9), 244-247.

Nattermann, L., Beyer, A., Ludewig, P., Hepp, T., Sterzer, E., & Volz, K. (2017). MOVPE growth of Ga(PBi) on GaP and GaP on Si with Bi fractions up to 8%. *Journal of Crystal Growth, 463*, 151–155.

Okamoto, H., & Oe, K. (1998). Growth of metastable alloy InAsBi by low-pressure MOVPE. *Japanese Journal of Applied Physics, 37*(3S), 1608.

Paulauskas, T., Pačebutas, V., Geižutis, A., Stanionytė, S., Dudutienė, E., Skapas, M., & Krotkus, A. (2020). GaAs 1-xBi x growth on Ge: Anti-phase domains, ordering, and exciton localization. *Scientific Reports, 10*(1), 1-12.

Penn, D. R. (1962). Wave-number-dependent dielectric function of semiconductors. *Physical Review, 128*(5), 2093-2100.

Perdew, J. P., Burke, K., & Ernzerhof, M. (1996). Generalized gradient approximation made simple. *Physical Review Letters, 77*(18), 3865-3868.

Perdew, J. P., Ruzsinszky, A., Csonka, G. I., Vydrov, O. A., Scuseria, G. E., Constantin, L. A., Zhou, X., & Burke, K. (2008). Restoring the density-gradient expansion for exchange in solids and surfaces. *Physical Review Letters, 100*(13), 136406.

Rahimi, S., Ebrahimi-Jaberi, R., Jalali-Asadabadi, F., Mollabashi, L., & Jalali-Asadabadi, S. (2022). Influence of (Ba, F) multidoping on structural, magnetic, optical, and electrical properties as well as performance enhancement of multiferroic BiFeO3. *Physical Review B, 106*(11), 115205.

Rajpalke, M. K., Linhart, W. M., Yu, K. M., Birkett, M., Alaria, J., Bomphrey, J. J., Sallis, S., Piper, L. F. J., Jones, T. S., Ashwin, M. J., & Veal, T. D. (2014). Bi-induced band gap reduction in epitaxial InSbBi alloys. *Applied Physics Letters, 105*(21), 212101.

Samajdar, D. P., & Dhar, S. (2016). Influence of Bi-related impurity states on the bandgap and spin-orbit splitting energy of dilute III-V-Bi alloys: InP1-xBix, InAs1-xBix, InSb1-xBix and GaSb1-xBix. *Superlattices and Microstructures, 89*, 112-119.

Slimani, H., Abid, H., & Benchehima, M. (2019). Prediction of optoelectronic properties for BexZnyCd1-x-ySe quaternary alloys: First-principles study. *Optik, 198*, 163288.

Tauc, J., Grigorovici, R., & Vancu, A. (1966). Optical properties and electronic structure of amorphous germanium. *Physica Status Solidi (b), 15*(2), 627-637.

Tran, F., & Blaha, P. (2009). Accurate band gaps of semiconductors and insulators with a semilocal exchange-correlation potential. *Physical Review Letters, 102*(22), 226401.

Usman, M. (2019). Towards low-loss telecom-wavelength photonic devices by designing GaBixAs1-x/Ga As core-shell nanowires. *Nanoscale, 11*(42), 20133-20143.

Usman, M., Broderick, C. A., Lindsay, A., & O'Reilly, E. P. (2011). Tight-binding analysis of the electronic structure of dilute bismide alloys of GaP and GaAs. *Physical Review B, 84*(24), 245202.

Vurgaftman, I., Meyer, J. R., & Ram-Mohan, L. R. (2001). Band parameters for III-V compound semiconductors and their alloys. *Journal of Applied Physics, 89*(11), 5815–5875.

Wang, K., Gu, Y., Zhou, H., Zhang, L., Kang, C., Wu, M., & Pan, W. (2014). InPBi single crystals grown by molecular beam epitaxy. *Scientific Reports, 4*(1), 5449.

Wang, S., & Lu, P. (2019). *Bismuth-containing alloys and nanostructures*. Springer.

Wang, S., & Ye, H. (2002). Plane-wave pseudopotential study on mechanical and electronic properties for IV and III-V crystalline phases with zinc-blende structure. *Physical Review B, 66*(23), 235111.

Wu, X., Chen, X., Pan, W., Wang, P., Zhang, L., Li, Y., Zhou, H., & Wang, K. (2016). Anomalous photoluminescence in InP1-xBix. *Scientific Reports, 6*(1), 1-8.

Wu, Z., & Cohen, R. E. (2006). More accurate generalized gradient approximation for solids. *Physical Review B, 73*(23), 235116.

Wyckoff, R. (1986). *Crystal structures* (2nd ed.). Krieger.

Yang, H., Song, T., Liang, X., & Zhao, G. (2015). First-principle study of the electronic band structure and the effective mass of the ternary alloy GaxIn1-xP. *Journal of Physics: Conference Series, 586*, 012048.

Zhang, X., Zhang, Y., Yue, L., Liang, H., Chi, C., Wu, Y., & Dai, L. (2019). Growth and properties of AlSbBi thin films by molecular beam epitaxy. *Journal of Alloys and Compounds, 801*, 239-242

Zunger, A., Wei, S.-H., Ferreira, L. G., & Bernard, J. E. (1990). Special quasirandom structures. *Physical Review Letters, 65*(3), 353-356.

Author(s) Information

Malika Tehami
Djillali Liabes University of Sidi Bel Abbes
Electronic's Department, Sidi Bel Abbes, Algeria
Contact e-mail: *mtehami2001@gmail.com*

Miloud Benchehima
University of Sciences and Technology Mohamed Boudiaf,
Electronic's Department, Oran, Algeria

Hamza Abid
Djillali Liabes University of Sidi Bel Abbes
Electronic's Department, Sidi Bel Abbes, Algeria

To cite this article:

Tehami, M., Benchehima, M., & Abid, H. (2025). Computational materials design: Tuning optoelectronic response in GaxIn1-xBiyP1-y alloys via structural matching to InP. *The Eurasia Proceedings of Science, Technology, Engineering & Mathematics, (EPSTEM) 38,* 226-243